Available online at www.sciencedirect.com
ScienceDirect
Trans. Nonferrous Met. Soc. China 34(2024) 1734−1744
Transactions of Nonferrous Metals Society of China
www.tnmsc.cn

First-principles insights into solute partition among various nano-phases in Al−Cu−Li−Mg alloys

Zheng-qing LIU[1,2], Yong JIANG[1,2,3], Yi-ren WANG[1], Jian-gang YAO[2]

1. School of Materials Science and Engineering, Central South University, Changsha 410083, China;
2. School of Materials Science and Engineering, Yantai Nanshan University, Yantai 265713, China;
3. State Key Laboratory of Powder Metallurgy, Central South University, Changsha 410083, China

Received 24 December 2022; accepted 16 May 2023

Abstract: First-principles energetics calculations were performed over a group of 25 candidate elements, to investigate their partition energies and behaviors among major nano-phases (δ'-Al_3Li, θ'-Al_2Cu, T_1-$Al_6Cu_4Li_3$ and S-Al_2CuMg) in most commercial Al−Cu−Li−Mg alloys. It was revealed that principal alloying element Li cannot directly affect θ' and S, Cu cannot directly affect δ', Mg cannot directly affect θ' and δ' but can weakly partition into T_1. As for micro-alloying elements, Si is the only element that can partition into all the four nano-phases. Au can partition into δ', θ' and S. Cd can partition into δ', T_1 and S. Zr can partition into δ' and T_1. Ni substitution can weakly partition into θ' and S. Ti, V, Zn, Ag and Mo can partition into δ' only. Cr, Mn, Fe and Co cannot directly affect any of the four nano-phases. Almost all RE-elements can strongly partition into T_1, δ' and S, but would be expelled by θ'. Only Sc is somehow particular to S, showing no partition preference in S. The newly obtained fundamental results could constitute a simple prototype database in support for the accelerated design of Al−Li based alloys and other related Al alloys.
Key words: Al−Cu−Li−Mg alloy; nano-phase; micro-alloying; solute partition; first-principles

1 Introduction

Al−Li based alloys have been widely used in weight-critical structural components in aircraft, aerospace and military applications, due to their excellent combination of low mass density, high specific stiffness and strength, and superior low-temperature toughness [1,2]. Binary Al−Li alloys can be efficiently strengthened by the high density precipitation of fully coherent $L1_2$-$\delta'(Al_3Li)$ along the habit {100} planes. However, due to the low interface strain and low interface energy, δ' can be easily sheared by dislocations via planar slip, leading to severe strain localization and hence a poor ductility [2,3].

The addition of principal alloying element Cu can induce various Cu-rich nano-phases, such as GP-zone($Al_{2x+1}Cu$, $x\geq2$), θ''(GP-II or Al_3Cu), $\theta'(Al_2Cu)$, $\theta(Al_2Cu)$, $T_1(Al_2CuLi)$, and/or $T_2(Al_6CuLi_3)$, depending on the atomic ratio of Cu/Li [4−6]. The co-precipitation of $\theta''/\theta'/\theta$ and T_1 along different habit planes of {100} and {111} can favorably alleviate strain localizations under deformation, so as to achieve more uniform strengthening effects in Al−Cu−Li alloys. Among these Cu-rich nano-phases, stable T_1 and metastable θ' are dominant in number popularity in peak aging [7,8]. θ' has a tetragonal structure (a=4.04 Å and c=5.80 Å) with a nominal composition of Al_2Cu, which is also highly coherent with the Al matrix along the habit plane {100} [9]. There are still considerable controversies about the atomic composition and atomic structure of T_1 [10−16]. Recently, KIM et al [13] examined

Corresponding author: Yong JIANG, E-mail: yjiang@csu.edu.cn
DOI: 10.1016/S1003-6326(24)66503-9

a group of five candidate structural models of T_1 that have been previously proposed using first-principles energetics calculations. Their results suggested that none of these T_1 model structures could be possibly thermodynamically stable, but have a tendency to decompose into Al_2Cu and Al_3Li. By their calculations, they proposed a new structural model of T_1 which can be more energy-favored. Only years later, the new structure model of T_1 phase has been further optimized by the same group [14]. The new improved model has a stoichiometric composition of $Al_6Cu_4Li_3$ with a hexagonal symmetry, corresponding to an orthorhombic supercell with the lattice constants of a=4.941 Å, b=8.641 Å, and c=9.232 Å.

Further co-alloying with Mg induces S' and/or S (Al_2CuMg) in Al−Cu−Li−Mg alloys, which can help reduce the detrimental precipitation-free zones (PFZs) at grain boundaries [17]. Historically, three different crystal structures have been proposed for S phase in the literature, namely the PW model [18], the Mondolfo model [19] and the RK model [20]. A high-angle annular dark-field scanning transmission electron microscopic (HAADF-STEM) study, in combined with first-principles calculations, suggested that only the PW model could be the possibly reasonable structure for describing S phase in Al−Cu−Mg alloys, and that the PW model has an orthorhombic structure of a=4.01 Å, b=9.29 Å, and c=7.14 Å [21].

Besides the principal alloying elements Cu and Mg, some micro-alloying elements have been often introduced into current generation commercial Al−Cu−Li−Mg alloys, showing profound influence on the formation and regulation of nano-phases and the microstructures. A dilute addition of Zr and/or Sc can favorably refine the grains and produce $L1_2$ type nano-phases [22−24]. These phases often precipitate earlier at higher temperature and can interact with later-precipitated $L1_2$-Al_3Li at lower temperatures in many ways, such as, by forming $L1_2$-Al(Li,Sc,Zr) nano-particles [25] and/or developing associated nano-complexes [26]. Ag micro-alloying can induce the formation of Mg−Ag atomic-clusters which can attract Cu and Li atoms to promote the nucleation of T_1 [27]. Zn micro-alloying may also benefit to modulating the electric-chemical potential of T_1 phase by substituting Cu in T_1, in favor for the improved anti-corrosion performance of Al−Cu−Li−Mg alloys [28].

It is natural to deduce that there may exist many other elements with promises for uses as principal- and micro-alloying elements in Al−Cu−Li−Mg alloys. They may have different potentials for affecting various nano-phases existing in the alloys, either by dissolving into their bulk-phase lattices via substitution or by segregating to their interfaces [29,30]. Knowledge about solute interaction with various nano-phases is of fundamental importance to multi-element Al−Li-based alloy designs, which, however, is still missing. Herein, we performed an extensive first-principles density functional theory (DFT) study over a group of 25 candidate elements, to investigate their partition preference among various nano-phases of Al−Cu−Li−Mg alloys from the energetics perspective.

2 Computational method

All the structural relaxation and energetics calculations were performed using the plane-wave DFT code − VASP (Vienna Ab initio Simulation Package) with periodic boundary conditions [31]. The ion-electron interaction was described by the Blöchl projector augmented wave method (PAW) within the frozen-core approximation as implemented in VASP [32]. The pseudopotential generated within the generalized gradient approximation (GGA) of Perdew–Burke–Ernzerhof (PBE) was used for the exchange–correlation functionals [33]. A sufficiently high energy cutoff of 400 eV was used for the plane-wave basis set expansion. For each bulk phase, the Monkhorst-Pack K-mesh for Brillouin-zone integrations was determined by achieving the total energy convergence of within 1 meV/atom. The ground-state atomic structures were optimized by minimizing the Hellmann-Feynman forces until the total forces on each ion were converged to within 0.01 eV/Å.

3 Results and discussion

3.1 Bulk properties of nano-phases

We first calculated the ground-state bulk structures and formation energies of δ'-Al_3Li, θ'-Al_2Cu, T_1-$Al_6Cu_4Li_3$ and S-Al_2CuMg phases in most commercial Al−Cu−Li−Mg alloys. T_1 and S structures were modeled as proposed by NA

et al [14] and PERLITZ et al [18], respectively. Figure 1 schematically shows the unit cells of δ', θ', T_1 and S phases for our calculations. The lattice constants and bulk moduli were optimized by fitting the total energy vs volume data to the universal binding-energy relation [34], and are compared with available experimental measurements [13,21,35−38] in Table 1. The maximum deviations of lattice constants and bulk moduli from the experiments are found within ~1% and 10%, suggesting a favorable agreement with experiments.

The formation energy can be calculated as

$$\Delta E=\frac{1}{N_A+N_B+N_C}(E_{tot}-N_A\mu_A-N_B\mu_B-N_C\mu_C) \quad (1)$$

where E_{tot} is the total energy of a fully relaxed unit cell, N_A, N_B and N_C are the atom numbers of elements A, B and C in the unit cell, and μ_A, μ_B and μ_C are the chemical potentials of elements A, B and C in their pure bulk phase, respectively. The calculated formation energies are also tabulated in Table 1. No experimental results of formation energies are available for a direct comparison. It is shown that the formation energies (ΔE) of these phases are all negative, with an energy driving force to form, but the formation preference decreases in the order of $T_1>S>\theta'>\delta'$. It is noted that the formation energies are evaluated with respect to the solutes in their pure bulk states, and hence the preference order just reflects their formation in their free-standing bulk phases. In next section, we will re-evaluate their formation energies and preference with respect to the solutes in their dissolution states inside the Al matrix.

3.2 Solute partition of solute elements in strengthening phases

A total of 25 candidate solute elements were chosen to evaluate their possible partition among various nano-phases in Al−Cu−Li−Mg alloys. These elements include 4 main-group elements, 14 transition elements and 7 rare-earth elements. Among which, Li, Cu and Mg are the principal alloying elements of Al−Cu−Li−Mg alloys, Mn, Zn, Zr, Ag and Sc are already proposed as micro-alloying elements in some Al−Cu−Li−Mg alloys,

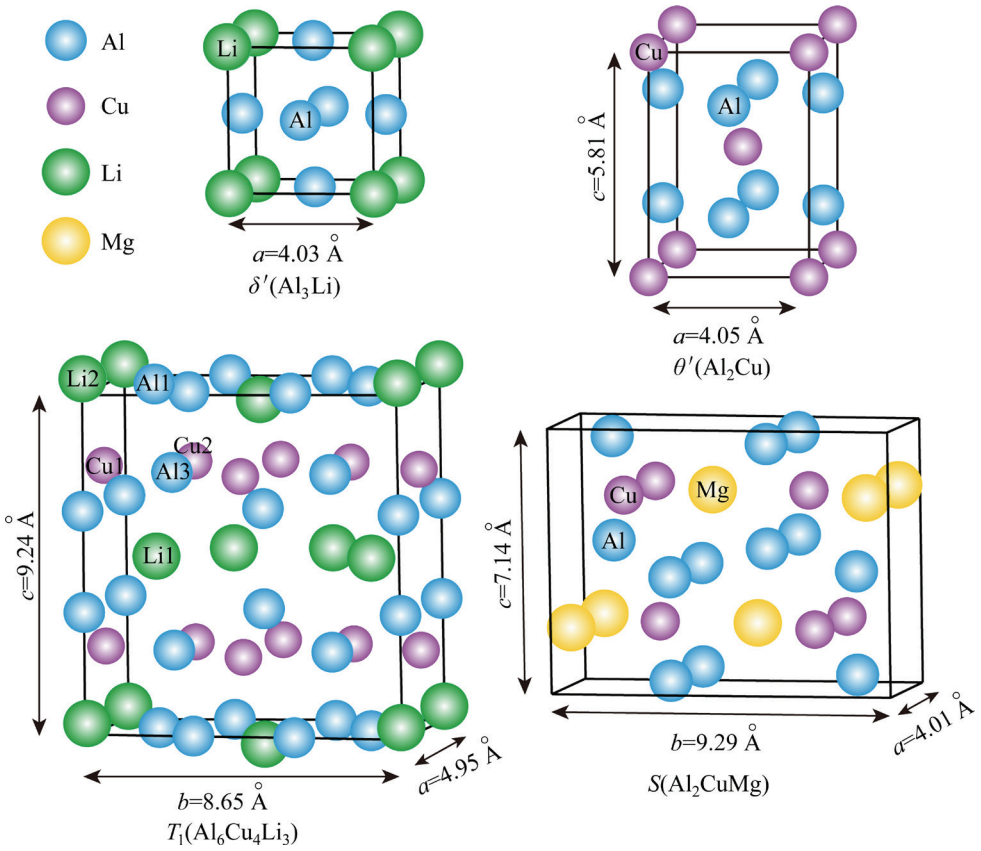

Fig. 1 Unit cell structures of δ'-Al_3Li, θ'-Al_2Cu, T_1-$Al_6Cu_4Li_3$ and S-Al_2CuMg phases (The possible substitutional sites are marked)

Table 1 Calculated bulk phase lattice constants, bulk moduli (B_0), and formation energies (ΔE) of Al and various nano-phases

Parameter	Al		Al_3Li (δ')		Al_2Cu (θ')	
	This work	Others	This work	Others	This work	Others
a/Å	4.040	4.040 [37]	4.026	4.028 [35]	4.092	4.08 [38]
c/Å	–	–	–	–	5.787	5.78 [38]
B_0/GPa	77.6	77.9 [37]	64.0	63.9 [35]	94.4	92.6 [39]
ΔE/(eV·atom^{-1})	–	–	−0.097	−0.097 [13]	−0.175	−0.175 [13]

Parameter	$Al_6Cu_4Li_3$ (T_1)		Al_2CuMg (S)	
	This work	Others	This work	Others
a/Å	4.948	4.941 [13]	4.004	4.01 [21]
b/Å	8.640	8.641 [13]	9.273	9.29 [21]
c/Å	9.233	9.232 [13]	7.144	7.14 [21]
B_0/GPa	79.6	–	74.9	75.2 [40]
ΔE/(eV·atom^{-1})	−0.240	−0.239 [13]	−0.183	−0.183 [36]

and Cd, Si and Au for some Al−Cu alloys. Some basic information of the 25 candidate solute elements is summarized in Table 2. It can be seen that the atom sizes of all the solute elements are fairly comparable to Al, and substitutional sites can be more favored than interstitial sites for solutes. Thus, for all these elements, only the substitutional sites will be considered in our subsequent calculations.

To calculate the partition energy of each element in one specific phase w.r.t in Al matrix, we constructed the sufficient large supercell for each phase based on the optimized lattice constant. The associated K-mesh setting for Brillouin-zone integrations was also optimized by total energy convergence tests. Eventually, we chose a 3×3×3 supercell of 108 atoms with a 4×4×4 K-mesh for pure Al and δ'-Al_3Li, a 3×3×2 supercell of 108 atoms with a 4×4×4 K-mesh for θ'-Al_2Cu, a 2×2×1 supercell of 52 atoms with a 5×6×5 K-mesh for T_1-$Al_6Cu_4Li_3$ and a 2×1×2 supercell of 64 atoms with a 5×5×3 K-mesh for S-Al_2CuMg, respectively. The solute partition energy (ΔE_{part}) of element X into a given phase is calculated as

$$E_{\text{part}}=(E^{\text{X}}_{\text{phase}}+E^{\text{perf}}_{\text{Al}})-(E^{\text{X}}_{\text{Al}}+E^{\text{perf}}_{\text{phase}}) \quad (2)$$

where $E^{\text{perf}}_{\text{phase}}$ and $E^{\text{X}}_{\text{phase}}$ are the total energies of the phase's supercell before and after solute substitution in the phase, and $E^{\text{perf}}_{\text{Al}}$ and E^{X}_{Al} are the total energies of the fcc-Al supercell before and after solute substitution in the Al matrix, respectively.

Figure 2 compares the calculated partition energies of all the possible solute elements in δ'-Al_3Li versus in the Al matrix. According to Eq. (2), only a negative ΔE_{part} predicts an energy-favored solute partition from the matrix into δ'. It is revealed in Fig. 2 that all the rare-earth elements can dissolve into δ'-Al_3Li by substituting the Li sites only, in attempt to retain the $L1_2$ structure in the form of $L1_2$-Al_3(Li, RE). This is in good accordance with the strong formation tendency of $L1_2$-Al_3RE and even various core-shelled nano-complexes in Al [37,41−43]. Most other elements can only substitute at either the Al or the Li sites (but not both). Especially, solutes Si, Zn, Ag, Cd and Au can dissolve into δ'-Al_3Li by substituting the Al sites only. Ti, V, Zr and Mo, like all the rare-earth elements, can dissolve into δ'-Al_3Li by substituting the Li sites only. Solutes Mn, Fe, Co and Ni are, however, unlikely to partition into δ'-Al_3Li but prefer to stay in the Al matrix. Interestingly, the principal alloying elements Cu and Mg, as well as Cr, show no obvious partition preference between δ'-Al_3Li and the Al matrix. It can be inferred that Cu, Mg and Cr, altogether with the indissoluble elements Mn, Fe, Co and Ni, can hardly influence the nucleation and growth of δ'-Al_3Li in Al alloys.

Using the same method, the partition energies of all the possible solute elements in θ'-Al_2Cu versus in the Al matrix are calculated in Fig. 3. It is found that, in contrast to δ'-Al_3Li, almost all the

Table 2 Information of 25 candidate solute elements being considered

Element group	Element	Group number	Atomic number	Crystal structure	Atomic radius/Å	Valence configuration
Main-group element	Li	IA	3	bcc	1.57	$2s^1$
	Mg	IIA	12	hcp	1.60	$3s^2$
	Al	IIIA	13	fcc	1.43	$3s^23p^1$
	Si	IVA	14	diamond	1.18	$3s^23p^2$
Transition element	Ti	IVB	22	hcp	1.47	$3d^24s^2$
	V	VB	23	bcc	1.35	$3d^34s^2$
	Cr	VIB	24	bcc	1.29	$3d^54s^1$
	Mn	VIIB	25	bcc	1.37	$3d^54s^2$
	Fe	VIIIB	26	bcc	1.26	$3d^64s^2$
	Co	VIIIB	27	hcp	1.25	$3d^74s^2$
	Ni	VIIIB	28	fcc	1.25	$3d^84s^2$
	Cu	IB	29	fcc	1.28	$3d^{10}4s^1$
	Zn	IIB	30	hcp	1.37	$3d^{10}4s^2$
	Zr	IIIB	40	hcp	1.60	$4d^25s^2$
	Mo	VIB	42	bcc	1.40	$4d^55s^1$
	Ag	IB	47	fcc	1.44	$4d^{10}5s^1$
	Cd	IIB	48	hcp	1.52	$4d^{10}5s^2$
	Au	IB	79	fcc	1.44	$5d^{10}6s^1$
Rare earth element	Sc	IIIB	21	hcp	1.64	$3d^14s^2$
	Y	IIIB	39	hcp	1.82	$4d^15s^2$
	La	IIIB	57	d-hcp	1.88	$5d^16s^2$
	Ce	IIIB	58	fcc	1.82	$4f^15d^16s^2$
	Pr	IIIB	59	d-hcp	1.82	$4f^26s^2$
	Er	IIIB	68	hcp	1.75	$4f^{12}6s^2$
	Yb	IIIB	90	fcc	1.94	$4f^{14}6s^2$

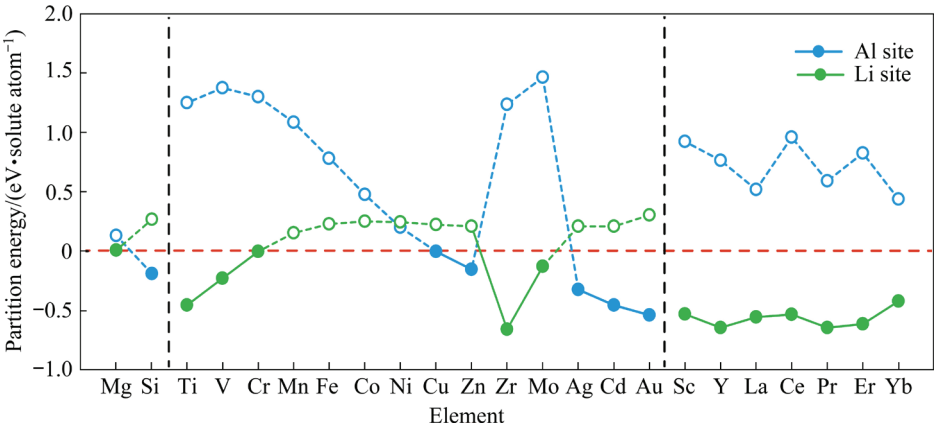

Fig. 2 Calculated partition energies of all solute elements in δ'-Al_3Li versus in Al matrix

solute elements have a positive partition energy in θ'(Al_2Cu). Thus, they would stay in the Al matrix in preference to enter θ' phase, with no ways to get involved directly into the nucleation and growth of θ'. Only a few elements (i.e. Si, Ni and Au) have been predicted with a very low (but non-zero) tendency of substituting Cu in θ'. There exist some previous experimental findings that favorably

support our calculations results. It has been reported that a trace addition of Au could influence the nucleation and growth of θ' by promoting a finer and more uniform distribution of θ' phases in an Al−Cu−Au alloy [44]. Si addition also resulted in finer lamellar eutectics of Al_2Cu+Si in an Al−Cu−Si alloy [45]. It is natural to deduce that Ni may also have some similar effects in the nucleation and growth of θ' in Al alloys.

Figure 4 compares the partition energies of all the possible solute elements in S-Al_2CuMg versus in the Al matrix. Most solute elements are unlikely to partition into S and thus can hardly affect its nucleation and growth in Al. All the rare-earth elements (only except Sc) can be strongly preferred to substitute Mg in S-Al_2CuMg. Solutes Si, Ni and Au, as well as Cd, are predicted with a very low (but non-zero) partition tendency to S-Al_2CuMg. Among which, Si and Cd have a very weak tendency to substitute Al, and Ni and Au have weak tendency to substitute Cu in S-Al_2CuMg. Experimental studies about the interaction of solutes and S-phase still lack, and are worth to be explored in future.

The partition energies of all the possible solute elements in T_1-Al_2CuLi phase are calculated in Fig. 5. The improved Kim's model has three non-equivalent Al sites (Al_1, Al_2, Al_3), two non-equivalent Cu sites (Cu_1, Cu_2) and two non-equivalent Li sites (Li_1, Li_2). The calculated ΔE_{part} are found to be very similar for all the solute elements substitution at the two Cu sites. They are predicted to be positive values or nearly zero, suggesting Cu sites are not preferred by any solute elements being considered here. The same trend is also revealed for almost all these elements at the three Al sites, except Si and Cd. In particular, Si can substitute all the Al sites while Cd tends to substitute the Al_2 sites only. All the rare-earth elements can strongly partition into T_1-Al_2CuLi phase, to substitute Li_2 sites more favorably than Li_1 sites. Mg, Zr and Cd can weakly partition into T_1. Mg prefer almost equally at Li_1 and Li_2 sites, Zr and Cr prefers Li_2 sites only. For a given element, by carefully comparing the ΔE_{part} values among different substitution sites, we can deduce a partition preference ordering of RE at Li > Si at Al > Zr at Li_2 ≈ Cd@Al_2/Li_2 > Mg@Li in T_1.

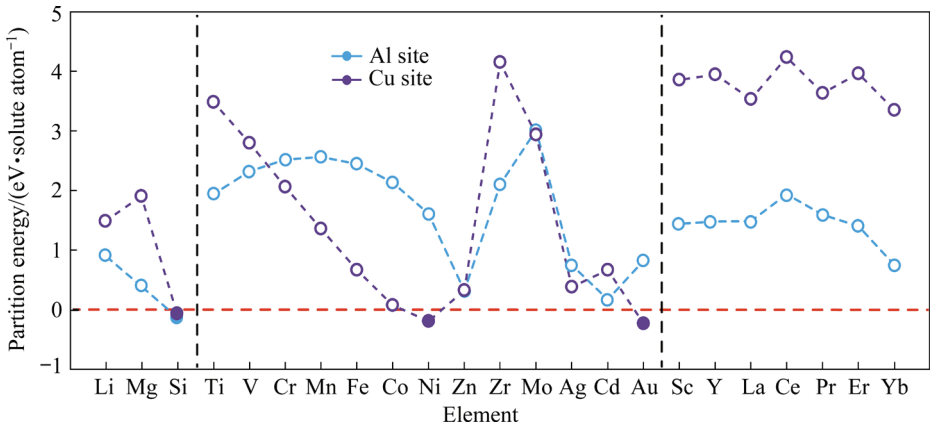

Fig. 3 Calculated partition energies of all solute elements in θ'-Al_2Cu versus in Al matrix

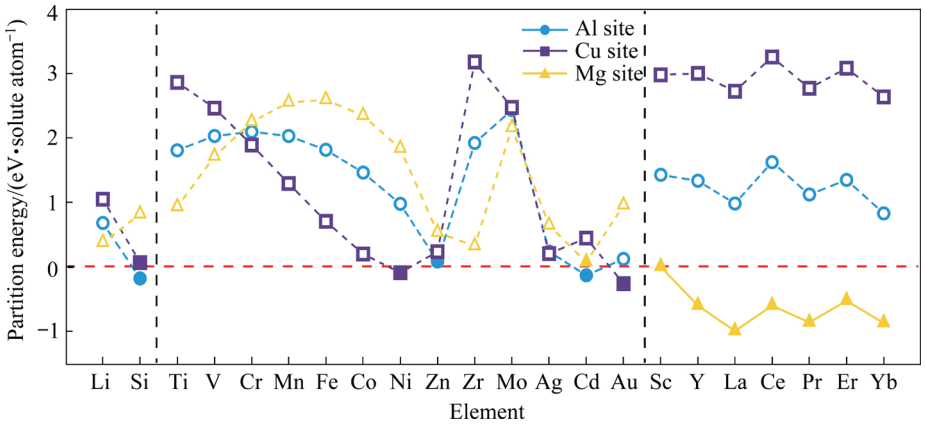

Fig. 4 Calculated partition energies of all solute elements in S-Al_2CuMg versus in Al matrix

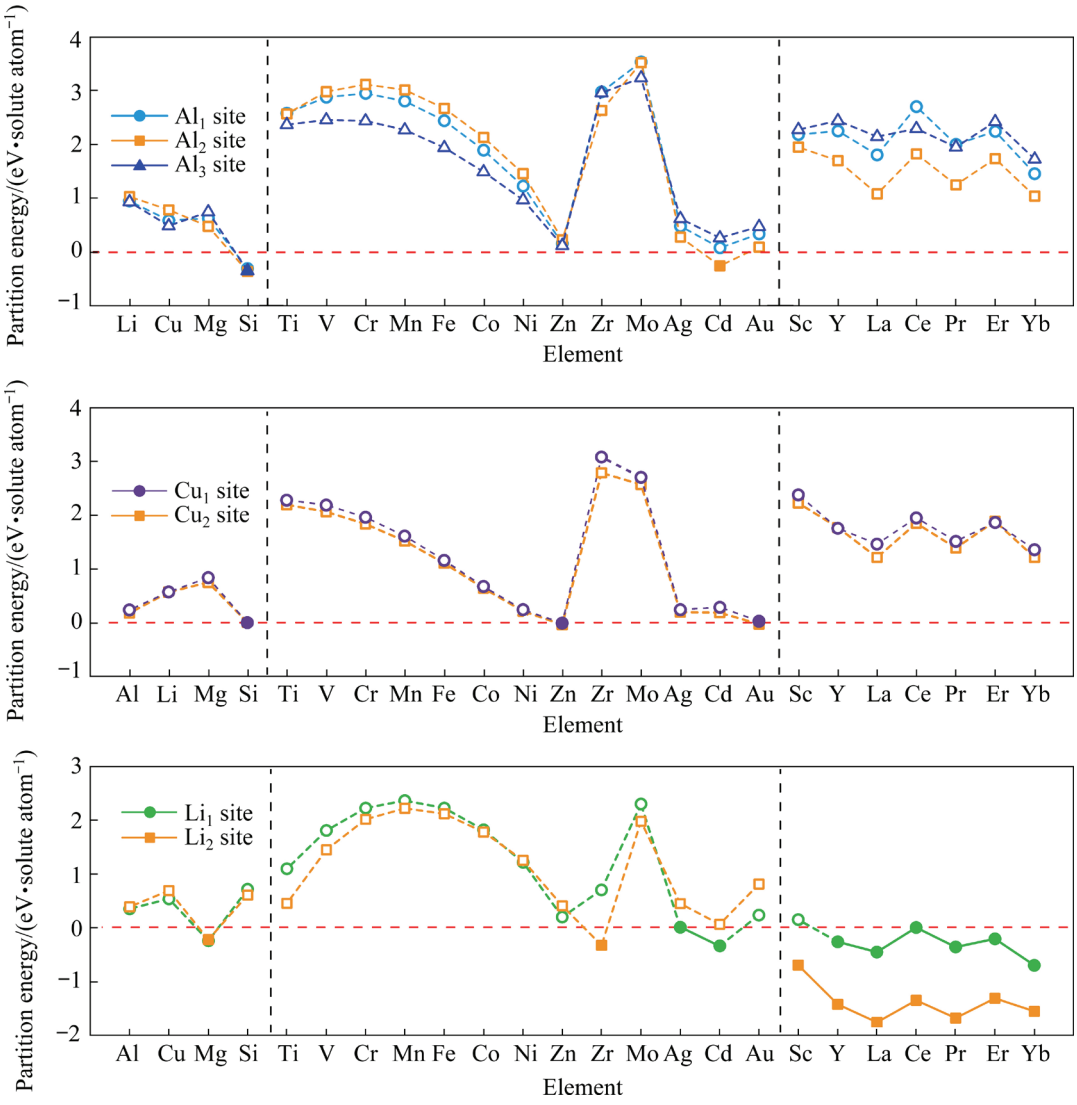

Fig. 5 Calculated partition energies of all solute elements in T_1-$Al_6Cu_4Li_3$ versus in Al matrix

So far, the partition preference of all the solute elements has been predicted for each individual nano-phase in commercial Al−Cu−Li−Mg alloys. Considering that all the partition energies are calculated using the same modeling and numerical methods, these energies can be directly used for predicting the solute partition behaviors and effects in multi-element Al−Cu−Li−Mg alloys. The following findings can be thus suggested: (1) Cu is a necessary element to form θ'-Al_2Cu, S-Al_2CuMg and T_1-Al_2CuLi, and excess Cu has no partition tendency to δ'-Al_3Li. Li is a necessary element to form δ' and T_1, but excess Li has no effects on nucleation of θ' and S. Mg is a necessary element to form S, and excess Mg may promote T_1 (by substituting Li sites); (2) Transition metal elements Ti, V, Mo, Ag, and Zn can only affect δ' by substituting Li sites. Zr can affect δ' and T_1 phases, with δ' being more preferred. Ni can equally weakly partition into θ' and S (by substituting Cu sites). Au can affect δ', θ' and S. Cd can partition into δ', S and T_1 with δ' being most preferred. Cr, Mn, Fe and Co can hardly partition into any of these phases; (3) All the RE elements can partition into δ', S and T_1 except Sc (Sc shows no partition preference to S), with T_1 being most preferred; (4) Si can affect all four type phases with δ' and T_1 being equally more favored.

For a better clarity, a four-set Venn's diagram is plotted in Fig. 6 to manifest our newly gained knowledge about the interaction between solutes and nano-phases. Each intersecting area indicates a group of solute elements that can partition into more than one nano-phase in Al−Cu−Li−Mg alloys.

The Venn's diagram in Fig. 6 accompanied with the calculated partition energies in Figs. 2−5 constitute a simple prototype database that can help in guiding the alloying design. For instance, for principal-alloying element design, a high Cu/Li ratio is favorable to increase the precipitation fractions of θ'-Al_2Cu, S-Al_2CuMg and T_1-Al_2CuLi with a minimal amount of δ'-Al_3Li. A high Mg/Li ratio is favorable to promote the nucleation of S and T_1 with a minimal amount of δ'. A sufficient Li content with low Cu and Mg contents would certainly favor δ' versus T_1, θ' and S, but for the sake of uniform strengthening, a careful micro-alloying design is critically demanded. Many δ'-only preferred elements, such as Ti, V, Zn, Ag and Mo, would better be excluded. Further to favor T_1 versus θ' and S, a sufficient Li content with Zr and Sc micro-alloying will be encouraged. Micro-alloying with Cd and other RE elements can favor T_1, but can promote θ'.

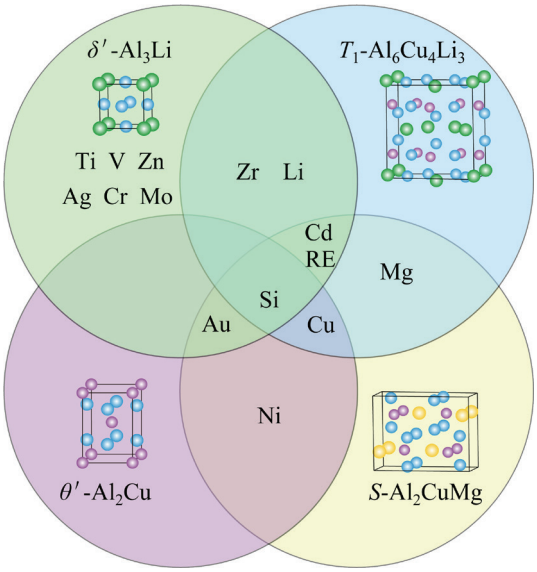

Fig. 6 Four-set Venn's diagram showing newly-gained knowledge about interaction between solutes and nano-phases in Al−Cu−Li−Mg alloys

To look back into the current-generation commercial Al−Cu−Li−Mg alloys, Zr, Zn, Ag and various RE elements have been often introduced as micro-alloying elements. Grain refinement effects induced by trace amounts of Zr and/or RE elements have been widely manifested in many experiments, which have been generally attributed to the earlier precipitated primary $L1_2$ phases (i.e. β'-Al_3Zr and/or various Al_3RE) at higher temperatures [46,47]. Our results further suggested that Zr may also promote the nucleation of T_1 but not θ' and S, and RE elements promote T_1, δ' and S but not θ'. As for Ag and Zn micro-alloying elements, they may promote δ' but cannot directly influence the nucleation of other phases. Nevertheless, we must note that, besides these bulk partition effects, all these solutes may possibly segregate to the interfaces of these phases which requires future investigation. A full clarification on micro-alloying mechanisms in Al−Cu−Mg−Li alloys also demands comprehensive grain boundary calculations, which have been largely dealt with in our previous study [48]. Furthermore, the possible roles of these elements on nano-phase interfaces will be our future major focus, to finally develop a full fundamental understanding of micro-alloying mechanisms in Al−Cu−Li−Mg alloys and other related Al alloys.

4 Conclusions

(1) Excess principal-alloying element Li cannot directly affect θ' and S, Cu cannot directly affect δ', Mg cannot directly affect θ' and δ' but can weakly partition into T_1.

(2) Although rather weakly, micro-alloying element Si is the only element that can partition into all the four nano-phases of θ', δ', S and T_1.

(3) For micro-alloying transition-metal elements, Au substitution is more favored in δ' than in θ' and S, but with no preference in T_1. Ni substitution can be weakly favored only in θ' and S. Cd substitution is more favored in δ' than in T_1 and S, but is forbidden in θ'. Zr substitution is more favored in δ' than in T_1, but is forbidden in θ' and S.

(4) For other micro-alloying transition-metal elements, Ti, V, Zn, Ag, and Mo can partition into δ' only. Cr, Mn, Fe and Co cannot directly affect any of the four nano-phases.

(5) All micro-alloying RE-elements can strongly partition into T_1, following by δ' and S, but would be expelled by θ'. Only Sc is somehow particular to S, showing no partition preference in S.

CRediT authorship contribution statement

Zheng-qing LIU: Conceptualization, Investigation, Validation, Data curation, Writing − Original draft; **Yong JIANG:** Project administration, Resources, Writing − Review & editing, Funding acquisition; **Yi-ren WANG:** Supervision, Resources; **Jian-gang YAO:** Investigation,

Validation, Data curation.

Declaration of competing interest

The authors declare that they have no known competing financial interests or personal relationships that could have appeared to influence the work reported in this paper.

Acknowledgments

The authors would like to thank for financial support from the National Science Foundation of China (No. 51971249), the Natural Science Foundation of Shandong Province, China (No. ZR2020KE012), and the Science and Technology Planning Project of Longkou City, China (No. 2021KJJH025). The computational resources at Hefei Advanced Computing Center and the High Performance Computing Center of Central South University are also highly appreciated.

References

[1] BETSOFEN S Y, ANTIPOV V V, KNYAZEV M I. Al−Cu−Li and Al−Mg−Li alloys: Phase composition, texture, and anisotropy of mechanical properties (Review) [J]. Russian Metallurgy (Metally), 2016, 2016: 326−341.

[2] EL-ATY A A, XU Yong-xu, GUO Xun-zhong, ZHANG Shi-hong, MA Yan, CHEN Da-yong. Strengthening mechanisms, deformation behavior, and anisotropic mechanical properties of Al−Li alloys: A review [J]. Journal of Advanced Research, 2018, 10: 49−67.

[3] RIOJA R J, LIU J. The evolution of Al−Li base products for aerospace and space applications [J]. Metallurgical and Materials Transactions A, 2012, 43: 3325−3337.

[4] PRASAD N E, RAMACHANDRAN T R. Phase diagrams and phase reactions in Al−Li alloys [M]//Aluminum−lithium Alloys. Boston: Butterworth-Heinemann, 2014: 61−97.

[5] LI Jin-feng, HUANG Jia-lei, LIU Dan-yang, CHEN Yong-lai, ZHANG Xu-hu, MA Peng-cheng. Distribution and evolution of aging precipitates in Al−Cu−Li alloy with high Li concentration [J]. Transactions of Nonferrous Metals Society of China, 2019, 29: 15−24.

[6] MA Yun-long, LI Jin-feng, ZHANG Run-zhe, TANG Jian-guo, HUANG Cheng, LI Hong-ying, ZHENG Zi-qiao. Strength and structure variation of 2195 Al−Li alloy caused by different deformation processes of hot extrusion and cold-rolling [J]. Transactions of Nonferrous Metals Society of China, 2020, 30: 835−849.

[7] GAYLE F W, HEUBAUM F H, PICKENS J R. Structure and properties during aging of an ultra-high strength Al−Cu−Li−Ag−Mg alloy [J]. Scripta Metallurgica et Materialia, 1990, 24: 79−84.

[8] ZHAO Xin-yue, LIU Wen-sheng, XIAO Dai-hong, MA Yun-zhu, HUANG Lan-ping, TANG Ya. A critical review: Crystal structure, evolution and interaction mechanism with dislocations of nano precipitates in Al−Li alloys [J]. Materials & Design, 2022, 217: 110629.

[9] ZHENG Yun-he, LIU Yi-xian, WILSON N, LIU Shi-qi, ZHAO Xiao-jun, CHEN Hou-wen, LI Jin-feng, ZHENG Zi-qiao, BOURGEOIS L, NIE Jian-Feng. Solute segregation induced sandwich structure in Al−Cu(−Au) alloys [J]. Acta Materialia, 2020, 184: 17−29.

[10] van SMAALEN S, MEETSMA A, DE BOER J L, BRONSVELD P M. Refinement of the crystal structure of hexagonal Al_2CuLi [J]. Journal of Solid State Chemistry, 1990, 85: 293−298.

[11] DWYER C, WEYLAND M, CHANG L Y, MUDDLE B C. Combined electron beam imaging and ab initio modeling of T_1 precipitates in Al−Li−Cu alloys [J]. Applied Physics Letters, 2011, 98: 201909.

[12] DONNADIEU P, SHAO Y, de GEUSER F, BOTTON G A, LAZAR S, CHEYNET M, de BOISSIEU M, DESCHAMPS A. Atomic structure of T_1 precipitates in Al−Li−Cu alloys revisited with HAADF-STEM imaging and small-angle X-ray scattering [J]. Acta Materialia, 2011, 59: 462−472.

[13] KIM K, ZHOU Bi-cheng, WOLVERTON C. First-principles study of crystal structure and stability of T_1 precipitates in Al−Li−Cu alloys [J]. Acta Materialia, 2018, 145: 337−346.

[14] NA B, ZHOU Bi-cheng, WOLVERTON C, KIM K. First-principles calculations of bulk and interfacial thermodynamic properties of the T_1 phase in Al−Cu−Li alloys [J]. Scripta Materialia, 2021, 202: 114009.

[15] HUANG J C, ARDELL A J. Crystal structure and stability of T_1 precipitates in aged Al−Li−Cu alloys [J]. Materials Science and Technology, 1987, 3: 176−188.

[16] HOWE J M, LEE J, VASUDÉVAN A K. Structure and deformation behavior of T_1 precipitate plates in an Al−2Li−1Cu alloy [J]. Metallurgical Transactions A, 1988, 19: 2911−2920.

[17] LEQUEU P, SMITH K P, DANIÉLOU A. Aluminum-copper-lithium alloy 2050 developed for medium to thick plate [J]. Journal of Materials Engineering and Performance, 2010, 19: 841−847.

[18] PERLITZ H, WESTGREN A. The crystal structure of Al_2CuMg [J]. Arkiv foer Kemi Mineralogi och Geologi, 1943, 16: 1−5.

[19] MONDOLFO L F. Aluminum alloy: Structure and properties [M]. London: Butterworth, 1976: 566−575.

[20] RADMILOVIC V, KILAAS R, DAHMEN U, SHIFLET G J. Structure and morphology of *S*-phase precipitates in aluminum [J]. Acta Materialia, 1999, 47: 3987−3997.

[21] LIU Z R, CHEN J H, WANG S B, YUAN D W, YIN M J, WU C L. The structure and the properties of *S*-phase in AlCuMg alloys [J]. Acta Materialia, 2011, 59: 7396−7405.

[22] RADMILOVIC V, TOLLEY A, MARQUIS E A, ROSSELL M D, LEE Z, DAHMEN U. Monodisperse Al_3(LiScZr) core/shell precipitates in Al alloys [J]. Scripta Materialia, 2008, 58: 529−532.

[23] MA Yun-long, LI Jin-feng, SANG Feng-jian, LI Hong-ying, ZHENG Zi-qiao, HUANG Cheng. Grain structure and tensile property of Al−Li alloy sheet caused by different cold rolling reduction [J]. Transactions of Nonferrous Metals

Society of China, 2019, 29: 1569−1582.

[24] YANG Qing-bo, DENG Yan-jun, YANG Mou, ZHANG Zhi-qing, LI Wei-guo, LIU Qing. Effect of Al_3Zr particles on hot-compression behavior and processing map for Al−Cu−Li based alloys at elevated temperatures [J]. Transactions of Nonferrous Metals Society of China, 2020, 30: 872−882.

[25] RADMILOVIC V, OPHUS C, MARQUIS E A, ROSSELL M D, TOLLEY A, GAUTAM A, ASTA M, DAHMEN U. Highly monodisperse core−shell particles created by solid-state reactions [J]. Nature Materials, 2011, 10: 710−715.

[26] LIU Zheng-qing, MA Pei-pei, JIANG Yong, WANG Yi-ren, LIU Chun-hui. First-principles insights into complex interplays among nano-phases in an Al−Cu−Li−Zr alloy [J]. Acta Materialia, 2022: 239: 118304.

[27] HUANG B P, ZHENG Z Q. Independent and combined roles of trace Mg and Ag additions in properties precipitation process and precipitation kinetics of Al−Cu−Li−(Mg)−(Ag)−Zr−Ti alloys [J]. Acta Materialia, 1998, 46: 4381−4393.

[28] GUMBMANN E, LEFEBVRE W, de GEUSER F, SIGLI C, DESCHAMPS A. The effect of minor solute additions on the precipitation path of an Al−Cu−Li alloy [J]. Acta Materialia, 2016, 115: 104−114.

[29] YAO Jian-gang, PAN Rong-kai, JIANG Yong, YIN Deng-feng, WANG Hua. Cu segregation at α-Al(111)/δ'-Al_3Li(111) interface [J]. The European Physical Journal B, 2018, 91: 239−244.

[30] GUMBMANN E, de GEUSER F, SIGLI C, DESCHAMPS A. Influence of Mg, Ag and Zn minor solute additions on the precipitation kinetics and strengthening of an Al−Cu−Li alloy [J]. Acta Materialia, 2017, 133: 172−185.

[31] KRESSE G, FURTHMÜLLER J. Efficient iterative schemes for ab initio total-energy calculations using a plane-wave basis set [J]. Physical Review B: Condensed Matter and Materials Physics, 1996, 54: 11169−11186.

[32] KRESSE G, JOUBERT D. From ultrasoft pseudopotentials to the projector augmented-wave method [J]. Physical Review B, 1999, 59: 1758−1775.

[33] PERDEW J P, BURKE K, ERNZERHOF M. Generalized gradient approximation made simple [J]. Physical Review Letters, 1996, 77: 3865−3868.

[34] MURNAGHAN F D. The compressibility of media under extreme pressures [J]. Proceedings of the National Academy of Sciences of the United States of America, 1944, 30: 244−247.

[35] YAO Jian-gang, ZHANG Chao-min, JIANG Yong, TAO Hui-jin, YIN Deng-feng. Prediction on elastic properties of off-stoichiometric L12-Al_3Li intermetallic due to point defects [J]. Computational Materials Science, 2015, 107: 184−189.

[36] ZHANG Yi-xin, WANG Yong-xin, CHEN Zheng, SUN Dong-qiang. Thermodynamics and elastic properties of precipitates with orthorhombic, hexagonal and cubic in Al−Li−Cu−Mg alloys [J]. International Journal of Metallurgy and Metal Physics, 2018, 3: 1−8.

[37] ZHANG Chao-min, JIANG Yong, CAO Fu-hua, HU Tao, WANG Yi-ren, YIN Deng-feng. Formation of coherent, core-shelled nano-particles in dilute Al−Sc−Zr alloys from the first-principles [J]. Journal of Materials Science & Technology, 2019, 35: 930−938.

[38] WOLVERTON C, OLOLINŠ V. Entropically favored ordering: The metallurgy of Al_2Cu revisited [J]. Physical Review Letters, 2001, 86: 5518−5521.

[39] OUYANG Y F, CHEN H M, TAO X M, GAO F, PENG Q, DU Y. A first-principles study of the structural, mechanical and electronic properties of precipitates of Al_2Cu in Al−Cu alloys [J]. Physical Chemistry Chemical Physics, 2018, 20: 967−976.

[40] LEFEBVRE W, MASQUELIER N, HOUARD J, PATTE R, ZAPOLSKY H. Tracking the path of dislocations across ordered Al_3Zr nano-precipitates in three dimensions [J]. Scripta Materialia, 2014, 70: 43−46.

[41] ZHANG Chao-min, YIN Deng-feng, JIANG Yong, WANG Yi-ren. Precipitation of L12-phase nano-particles in dilute Al−Er−Zr alloys from the first-principles [J]. Computational Materials Science, 2019, 162: 171−177.

[42] ZHANG Chao-min, JIANG Yong, GUO Xiu-hua, SONG Ke-xing. Formation and relative stabilities of core-shelled L12-phase nano-structures in dilute Al−Sc−Er alloys [J]. Acta Metallurgica Sinica (English Letters), 2020, 33: 1627−1634.

[43] ZHANG Chao-min, XIE Pan, JIANG Yong, ZHAN Sheng, MING Wen-quan, CHEN Jiang-hua, SONG Ke-xing, ZHANG Hao. Double-shelled L12 nano-structures in quaternary Al−Er−Sc−Zr alloys: Origin and critical significance [J]. Acta Metallurgica Sinica (English Letters), 2021, 34: 1277−1284.

[44] CHEN Yi-qiang, ZHANG Ze-zhong, CHEN Zhen, TSALANIDIS A, WEYLAND M, FINDLAY S, ALLEN Leslie J, LI Jie-hua, MEDHEKAR N V, BOURGEOIS L. The enhanced theta-prime (θ') precipitation in an Al−Cu alloy with trace Au additions [J]. Acta Materialia, 2017, 125: 340−350.

[45] OSÓRIO W R, MOUTINHO D J, PEIXOTO L C, FERREIRA I L, GARCIA A. Macrosegregation and microstructure dendritic array affecting the electrochemical behaviour of ternary Al−Cu−Si alloys [J]. Electrochimica Acta, 2011, 56: 8412−8421.

[46] DORIN T, RAMAJAYAM M, LAMB J, LANGAN T. Effect of Sc and Zr additions on the microstructure/strength of Al−Cu binary alloys [J]. Materials Science and Engineering A, 2017, 707: 58−64.

[47] FAN Li, HAO Qi-tang, HAN Wen-ke. Dual characteristic of trace rare earth elements in a commercial casting Al−Cu−X alloy [J]. Rare Metals, 2015, 34: 308−313.

[48] TANG Jia-wei, WANG Yi-ren, JIANG Yong, YAO Jian-gang, ZHANG Hao. Solute segregation to grain boundaries in Al: A first-principles evaluation [J]. Acta Metallurgica Sinica (English Letters), 2022, 35: 1572−1582.

Al−Cu−Li−Mg 合金纳米相之间溶质配分行为的第一性原理研究

刘正卿[1,2]，江 勇[1,2,3]，王怡人[1]，姚建刚[2]

1. 中南大学 材料科学与工程学院，长沙 410083；
2. 烟台南山学院 材料科学与工程学院，烟台 265713；
3. 中南大学 粉末冶金国家重点实验室，长沙 410083

摘 要：采用一性原理计算考察 25 种合金化元素在大多数商业牌号 Al−Cu−Li−Mg 合金中主要纳米相(δ'-Al_3Li、θ'-Al_2Cu、T_1-$Al_6Cu_4Li_3$ 和 S-Al_2CuMg)之间的溶质配分能和配分行为。计算结果表明，主合金化元素 Li 不能直接影响 θ'和 S 相，Cu 不能直接影响 δ'相，Mg 不能直接影响 θ'和 δ'相，但可以较弱地固溶于 T_1 相。对于微合金化元素，Si 是唯一一种可以固溶于 4 种纳米相的元素。Au 能固溶于 δ'、θ'和 S 相，Cd 能固溶于 δ'、T_1 和 S 相，Zr 能固溶于 δ'和 T_1 相，Ni 仅有微弱的趋势固溶于 θ'和 S 相。Ti、V、Zn、Ag 和 Mo 只能固溶于 δ'相，而 Cr、Mn、Fe 和 Co 对这 4 种纳米相均没有直接影响。几乎所有的稀土元素均能强烈固溶于 T_1、δ'和 S 相，但无法固溶于 θ'相。仅 Sc 略显特殊，对 S 相没有明显的固溶趋势。计算预测的溶质配分能构成了一个原型数据库，有利于指导和加速 Al−Li 合金及其他相关 Al 合金的设计。

关键词：Al−Cu−Li−Mg 合金；纳米相；微合金化；溶质配分；第一性原理

(Edited by Xiang-qun LI)